

Behaviour of open beam-to-tubular column angle connections under combined loading conditions

Yanzhi Liu¹, Christian Málaga-Chuquitaype^{*2} and Ahmed Y. Elghazouli²

¹ College of Civil Engineering, Hunan University, China

² Department of Civil and Environmental Engineering, Imperial College London, UK

(Received April 04, 2013, Revised September 23, 2013, Accepted October 04, 2013)

Abstract. This paper examines the behaviour of two types of practical open beam-to-tubular column connection details subjected to combined moment, axial and/or shear loads. Detailed continuum finite element models are developed and validated against available experimental results, and extended to deal with flexural, axial and shear load interactions. A numerical investigation is then carried out on the behaviour of selected connections with different stiffness and strength characteristics under various load combination scenarios. The influence of applied levels of axial tensile or compressive loads on the bending stiffness and capacity is examined and discussed. Additionally, the interaction effects between shear forces and co-existing bending and axial loads are examined and shown to be comparatively insignificant in terms of stiffness and capacity in most cases. It is also shown that the range of connections considered in this paper can provide rotational ductility levels in excess of those required under typical design scenarios. Based on these findings, a simplified component-based representation is proposed and described, and its ability to represent the connection response under combined loading is verified using results from detailed numerical simulations.

Keywords: semi-rigid joints; blind-bolted angle connections; combined channel / angle connections; combined loading conditions; interaction curves

1. Introduction

The structural efficiency and architectural appeal of Hollow Structural Steel Sections (HSS) make them an effective choice as column members. However, the difficulties associated with the lack of access for installation of conventional bolts have often resulted in the under exploitation of the merits of HSS. The need for the development of practical and cost-effective solutions for connections to tubular members is also motivated by the relatively high costs associated with the construction, inspection and maintenance of fully welded details. Accordingly, recent research has focused on the development of a number of connection alternatives including blind-bolted and reverse channel details to tubular columns (France *et al.* 1999, Barnett *et al.* 2001, Ding and Wang 2007, Elghazouli *et al.* 2009, Málaga-Chuquitaype and Elghazouli 2010a, Lee *et al.* 2011, Tizani *et al.* 2013).

*Corresponding author, Ph.D., E-mail: c.malaga@imperial.ac.uk

Several experimental and analytical investigations have examined the behaviour of open beam-to-tubular column connections under a variety of loading conditions such as bending, direct tension, direct compression and shear actions (France *et al.* 1999, Elghazouli *et al.* 2009, Málaga-Chuquitaype and Elghazouli 2010a, Lee *et al.* 2011, Liu *et al.* 2012a, b, Tizani *et al.* 2013). Nevertheless, there are other loading situations that may involve a combination of two or more loading types acting simultaneously. Such situations may include the idealised scenario of a sudden column loss, where significant compressive arching and tensile catenary actions can be imposed on the connections within the removed column zone (Vlassis *et al.* 2008), or the case of floor-to-floor impact where the falling debris from the upper falling floors may result in significant shear loading on the connections either directly or as a result of dynamic effects (Vlassis *et al.* 2009). It has also been demonstrated (Elghazouli and Izzuddin 2000, 2001, Liu *et al.* 2002) that significant levels of concurrent axial and bending loads are induced in connections under fire conditions.

In order to further the understanding of the behaviour of blind-bolted connections, a number of experimental investigations have been carried out. Barnett *et al.* (2001) performed a review of different blind-bolting alternatives and carried out an experimental study on blind-bolted T-stubs and connections using Hollo-bolts. Elghazouli *et al.* (2009) performed an experimental investigation into the monotonic and cyclic behaviour of *top and seat* as well as *top, seat and web angle* connections Hollo-bolted to structural hollow columns. It was shown that the grade of the Hollo-bolt, coupled with the gauge distance between the Hollo-bolt and beam flange, have a most notable effect on the flexural response of this type of connection. Yeomans (1998) performed shear and tension tests to determine the capacity of Hollo-bolts and reported the failure shear load as a function of column thickness for Grade 8.8 M16 and M20 Hollo-bolts. Lee *et al.* (2011) presented experimental and analytical investigations on the bending response of blind-bolted connections to tubular columns with extended T-stubs and highlighted the stiffness enhancement provided by the additional channels connecting the T-stubs to a backplate attached to the hollow section column. Liu *et al.* (2012a, b) carried out experimental studies on blind-bolted angle connections subjected to direct axial and shear loading. A detailed characterisation of the full axial force-displacement and shear force-displacement relationships for Hollo-bolted angle connections to tubes was carried out and discussed. More recently, Tizani *et al.* (2013) performed six tests on connections between concrete filled tubular columns and open beams incorporating extended Hollo-bolts subjected to cyclic loading. It was shown that this connection can offer reasonable levels of capacity and ductility when adequate wall thicknesses and concrete strengths are selected.

The behaviour of reverse channel connections, which enable the use of normal bolts, has also been the subject of a number of experimental studies. Ding and Wang (2007) compared the fire resistance of four *end-plate* reverse channel connections with other open beam-to-filled tubular column connection details. This study concluded that reverse channel connections can offer the most favourable structural behaviour and cost-effectiveness among the different details considered. Málaga-Chuquitaype and Elghazouli (2010a) carried out an experimental study into the flexural behaviour of combined channel/angle connections including *top and seat* as well as *top, seat and web angle details* under monotonic and cyclic loading. It was observed that the flexibility of the reverse channel component as well as the angle gauge distance have a direct influence on both the initial rotational stiffness and moment capacity of the connection, and the main inelastic mechanisms exhibited by this type of connection were identified. Liu *et al.* (2012a, b) performed an experimental investigation on combined channel/angle connections under axial and shear loads. It was concluded that this connection can provide significant shear-ductility levels compared to

those observed in blind-bolted details.

Detailed finite element (FE) models for the simulation of blind-bolted or reverse channel joints with angles have also been proposed. Wang *et al.* (2010) developed theoretical representations as well as numerical models by means of the FE program ANSYS (2003) to investigate the tension behaviour of Holo-bolted T-stubs. The clamping and force transfer mechanisms of the Holo-bolt, together with the stiffness, strength and deformation capacity of the connections were examined. A detailed numerical model was also developed by Liu *et al.* (2012a, b) employing the FE program ABAQUS (2003). This model included a number of advanced modelling features such as loading reversal, contact phenomena, bolt slippage definition and bolt pretension application. The detailed numerical simulations provided a good agreement with previous experimental results in terms of stiffness, capacity and failure modes.

Analytical studies on the response prediction of bolted connections to tubular columns are limited despite the recognition that the local behaviour of the tubular column is significantly different from that of open sections. Ghobarah *et al.* (1996) suggested a model for the estimation of the initial stiffness and capacity of blind-bolted end-plate connections between open beams and tubular columns employing High Strength blind-bolts (Huck International Inc. 1990). Wang *et al.* (2010) investigated the behaviour of Holo-bolted T-stubs and proposed an analytical model for the evaluation of their initial stiffness. Málaga-Chuquitaype and Elghazouli proposed a component-based mechanical model able to trace the full monotonic and cyclic response of blind-bolted (Málaga-Chuquitaype and Elghazouli 2010b) as well as reverse channel (Málaga-Chuquitaype 2011) connections. Park and Wang (2012) derived and validated analytical expressions for predicting the initial stiffness in bolted endplate connections to tubes based on the component method. Liu *et al.* (2012a, b) extended the component-based method to deal with the response of open beam-to-tubular column connections with angles under shear actions as well as direct tension or compression loads.

It can be noted from the above discussion that although the response of semi-rigid connections to tubes under direct axial, shear or bending loading is reasonably well established, there is a comparative lack of research on the connection response under coexisting loading scenarios. Moreover, the current detailed European design guidance (CEN 2005), which adopts a comprehensive component approach, is applicable only when the axial force on the connection is less than 5% of the connected member design plastic resistance. Clearly, as noted previously, the axial force imposed on the joint could exceed this value under extreme loading conditions. To this end, only a limited number of experimental studies on the influence of the axial force on the bending capacity of connections have been carried out. Simoes da Silva *et al.* (2004) and De Lima *et al.* (2004) examined the effect of combined axial force and flexural demands on flush and extended end plate connection configurations. Yang *et al.* (2000) and Urbonas and Daniunas (2006) used FE analysis to investigate the behaviour of bolted angle connections subjected to combined shear-moment and combined axial force-bending actions. These studies focussed on bolted end-plate or bolted angle open beam-to-open column connections. There is nevertheless a need for a detailed characterisation of the behaviour of bolted connections to tubular columns under combined loading conditions.

This paper addresses the issues highlighted above using detailed numerical studies as well as simplified mechanical representations. Particular emphasis is given to the behaviour of blind bolted and reverse channel angle connections subjected to combined loading conditions. Firstly, confidence is established in the use of detailed FE models through validation against recent experimental results. Secondly, a numerical investigation is carried out on the behaviour of eight

selected connections with different stiffness and strength characteristics under various load combinations (e.g., bending, combined bending and axial loads, bending and shear loads, etc.). Finally, a component-based representation is proposed and validated against moment-axial relationships obtained from the numerical simulations.

2. Numerical modelling

Detailed three-dimensional (3D) models developed using the FE program ABAQUS V6.7 (2003) are employed in this paper to examine the connection response to the simultaneous application of different actions including: (i) axial and bending loads; (ii) shear and bending loads; and (iii) shear and axial loads. This model, illustrated in Fig. 1, makes use of eight-noded brick solid elements of Type C3D8I. Special attention was given to the faithful representation of the geometric and mechanical characteristics of the bolts including the shank, sleeve, head and nut, as depicted in Fig. 1. The stress-strain relationships for the material of all the connection components were defined by a tri-linear kinematic hardening representation with an elastic modulus of 210 GPa and a Poisson's ratio of 0.3. This steel stress-strain relationship incorporates an elastic stage, a constant stress plateau up to a strain level of approximately 0.01, and a 1% strain-hardening stiffness thereafter. The models consider the yield stress and ultimate strength values for the angle, beam and column components summarised in Table 1; these values are based on the mean values obtained from previous experimental investigations (Liu *et al.* 2012a).

Contact phenomena between pairs of interacting surfaces were taken into account by defining 'hard' and 'friction' surface interactions. The more flexible surface was chosen as 'slave', while the more rigid area was defined as 'master'. Slippage was considered by means of the standard ABAQUS contact definitions. To this end, a 'friction' surface was employed in the tangential direction with a friction coefficient of 0.3. Similarly, a 'hard' surface contact pressure over-closure relationship was defined in the normal direction to enforce no-overlapping between the contact surfaces. Bolt pretension in standard bolts and Holo-bolts was introduced by means of two loading steps. Firstly, pretension forces of 100 kN for Grade 10.9 M16 standard bolts and 60 kN for Grade 10.9 M16 Holo-bolts were applied. The second step involved removing the applied pretension force while simultaneously fixing the bolt length at its deformed (shortened) value.

A number of mesh sensitivity studies were carried out in order to arrive at an optimum representation which involves a comparatively finer mesh for the angles and bolts as well as the

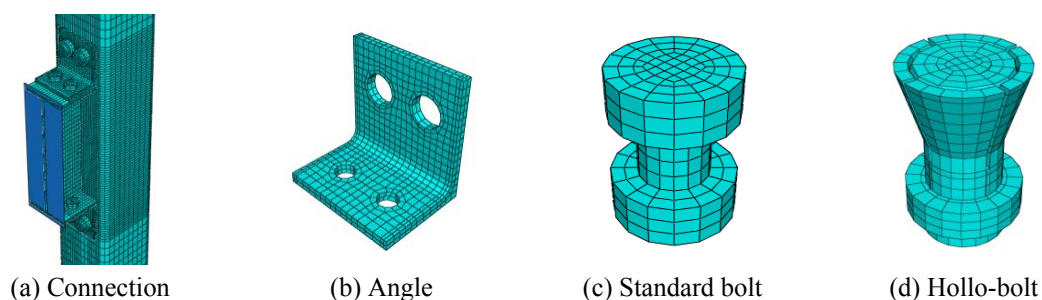


Fig. 1 Views of the finite element model

Table 1 Material properties of connection components

	Yield stress (N/mm ²)	Ultimate stress (N/mm ²)
UB 305 × 165 × 25	330	440
UB 305 × 102 × 25	400	490
SHS 200 × 200 × 10	430	490
SHS 150 × 150 × 10	340	430
SHS 150 × 150 × 6.3	390	490
L 100 × 75 × 8	310	440
L 100 × 80 × 15	290	450
Hollo-bolt sleeve	380	510

areas within the beams and columns which are in contact with these components, whereas a relatively coarser mesh was employed elsewhere. The dimensions of the adopted mesh ranged between 6 mm within the refined region and up to 100 mm within the coarser region.

This finite element model was validated against available experimental data (Elghazouli *et al.* 2009, Málaga-Chuquitaype and Elghazouli 2010a, Liu *et al.* 2012a, b). The dataset employed for validation purposes includes bending, direct axial and direct shear tests on both Hollo-bolted angle connections and reverse channel configurations. Fig. 2 depicts representative comparisons for a typical Hollo-bolted angle connection detail referred to as Specimen H10-N8-G50-T in Liu *et al.* (2012a); a more detailed account of the validation of these finite element models can be found elsewhere (Liu *et al.* 2012a, b).

As shown in Fig. 2, the finite element representations can simulate reasonably well the overall behaviour of bolted angle connections under various loading conditions. In particular, the stiffness, capacity and ultimate failure modes are all very well predicted. Close examination of the results of the numerical models enables the observation of key response characteristics, including the stress distribution and deformation patterns (Liu *et al.* 2012a, b). Accordingly, these validated numerical models are employed herein in order to assess the behaviour of semi-rigid open beam-to-tubular column connections with angles under combined loading conditions.

3. Response assessment

3.1 Connection details

Fig. 3 and Table 2 present eight typical connection configurations chosen in order to cover a wide range of stiffness and capacity values in order to assess the response of open beam-to-tubular column angle connections under combined loading. The first three configurations (H1, H2 and H3 in Table 2 and Fig. 3(a)), are blind-bolted *top and seat* angle details joining a universal beam (UB) 305 × 102 × 25 with a SHS 150 × 150 × 10 column in the case of Connections H1, H2 and a SHS 150 × 150 × 6.3 for Connection H3. A blind-bolted *top, seat and web angle* connection detail is also included (Fig 3(b)) which employs a universal beam (UB) 305 × 165 × 25 and a tubular column SHS 150 × 150 × 10. On the other hand, four combined channel/angle connections are considered (R1, R2, R3 and R4 in Table 2 and Figs. 3(c) - (d)). SHS 200 × 200 × 10 columns are

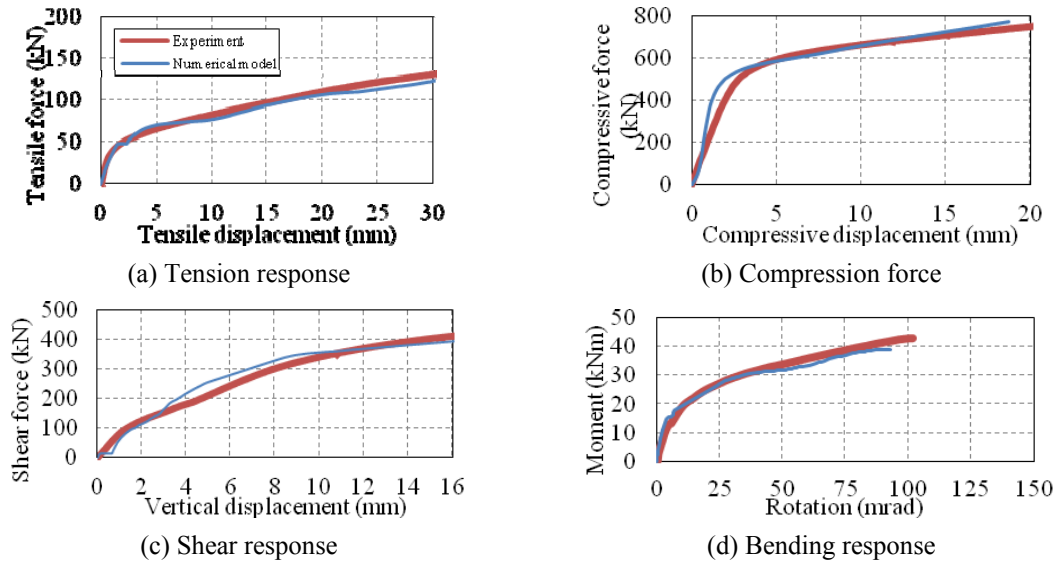


Fig. 2 Comparison of experimental and numerical response for a Holo-bolted angle connection (Specimen H10-N8-G50-T in Reference (Liu *et al.* 2012))

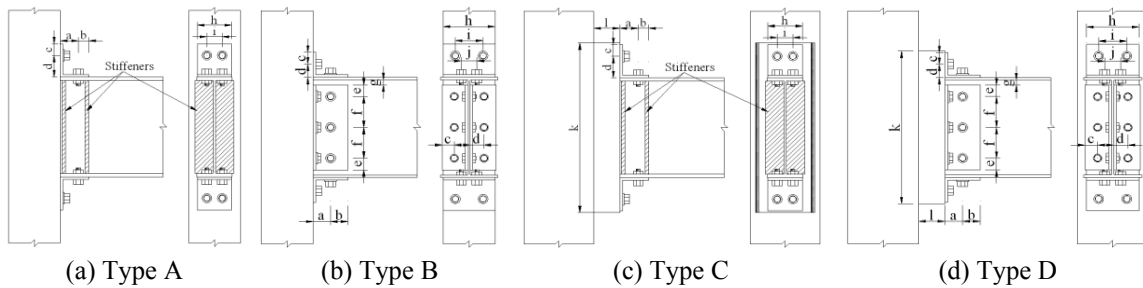


Fig. 3 Configuration of the selected connections

Table 2 Details of the selected connections

Type	Angle section	Channel section (cut from)	Dimensions in mm (as shown in Fig. 3)												
			a	b	c	d	e	f	g	h	i	j	k	l	
Blind-bolted angle connections															
H1	A	L 100×75×8	-	45	30	35	65	-	-	-	100	45	45	-	-
H2	A	L 100×75×8	-	50	50	35	40	-	-	-	100	45	45	-	-
H3	A	L 100×80×15	-	50	50	35	45	-	-	-	100	45	45	-	-
H4	B	L 100×75×8	-	50	50	35	40	35	95	12.5	150	80	45	-	-
Combined channel/angle connections															
R1	C	L 100×75×8	SHS 150×150×10	45	30	35	65	-	-	-	100	45	45	515	70
R2	C	L 100×75×8	SHS 150×150×10	50	50	35	40	-	-	-	100	45	45	465	70
R3	C	L 100×80×15	SHS 150×150×6.3	50	50	35	45	-	-	-	100	45	45	475	70
R4	D	L 100×75×8	SHS 150×150×10	50	50	35	40	35	95	12.5	150	80	45	465	70

employed in all reverse channel details while UB305 × 102 × 25 beams are used in Connections R1, R2 and R4 and UB305 × 165 × 25 are used in Connection R4. All geometric characteristics, as well as the corresponding angle and channel sizes, are summarised in Table 2. Grade 10.9 M16 standard bolts are used to connect the beam flange and angles, as well as the reverse channel and angle components, while Grade 10.9 M16 Holo-bolts are utilised between the tubular column and angles. The values of material yield and ultimate strengths of the angle, beam and column components correspond to those previously presented in Table 1.

As expected, the stiffness of the beam web can have a significant influence on the shear behaviour (Liu 2012). Local buckling of the beam web can prevent the connection from reaching its maximum shear capacity and initiate intricate localised effects in the beam. Therefore, in order to focus on the response of key connection components, beam web stiffeners were included to prevent premature local beam effects in the top and seat angle connections (Types A and C in Fig. 3). On the other hand, as the double web angles are stiff enough to prevent local buckling of the beam web, no additional stiffeners were employed in Connections H4 and R4 (Types B and D in Fig. 3) which incorporate double web angles.

3.2 Combined bending and axial loads

The influence of the axial force on the connection bending capacity (both yield and maximum), rotational stiffness and rotational capacity is depicted in Figs. 4-8. In these figures, the axial force (N) is normalised with respect to the connection axial yield capacities ($N_{y,t}$ or $N_{y,c}$, in tension or compression, respectively) or the corresponding connection maximum capacities ($N_{u,t}$ or $N_{u,c}$, in tension or compression, respectively). Similarly, the values of bending moment (M) are normalised with respect to the corresponding pure moment at yield ($M_{y,0}$) and pure maximum moment ($M_{u,0}$). The maximum connection capacity is defined herein as the peak action (axial force or moment) immediately before the occurrence of any strength degradation (e.g., due to localized damage). Furthermore, yield capacities are obtained from bi-linear idealizations of the corresponding action-deformation relationships (i.e., axial force-displacement for tension and compression or moment-rotation for bending). In all cases, the connections were subjected to initially-prescribed constant axial loads followed by applied moments.

3.2.1 Yield moment

Fig. 4 presents the interaction curves between the normalized moment capacity at yield

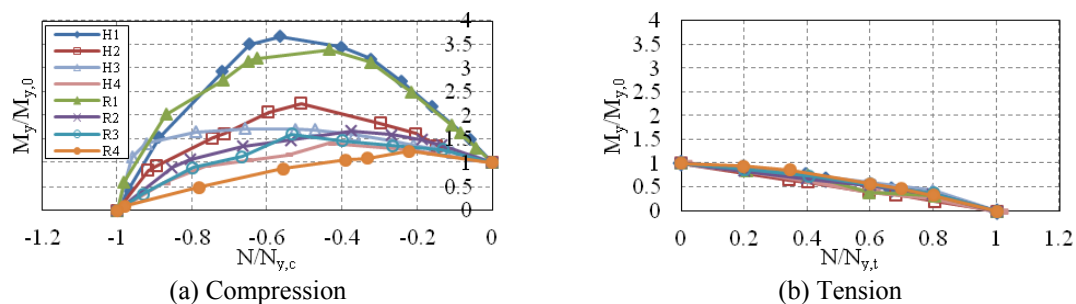
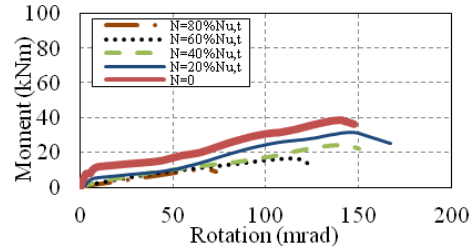
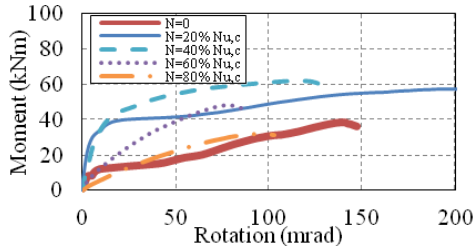
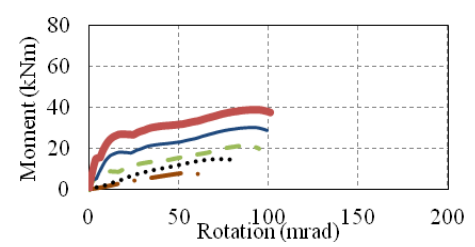
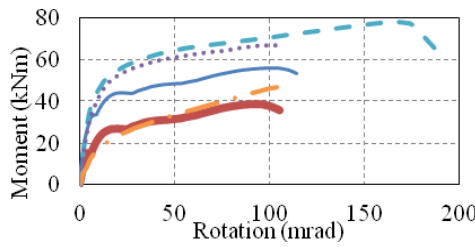


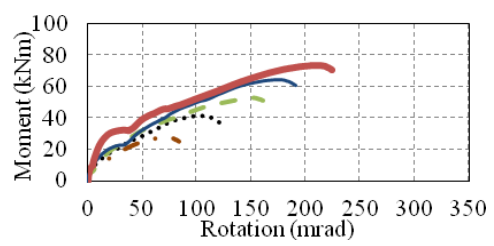
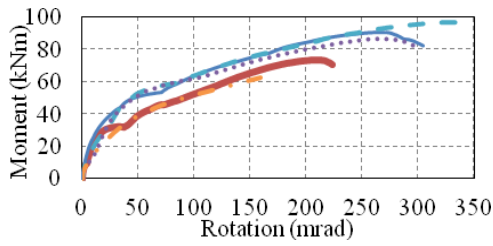
Fig. 4 Moment-axial interaction curves at yield



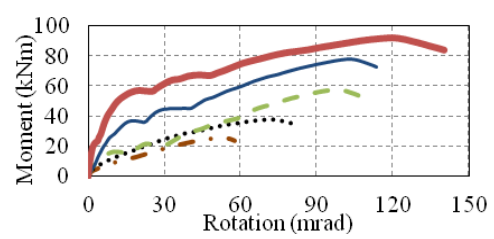
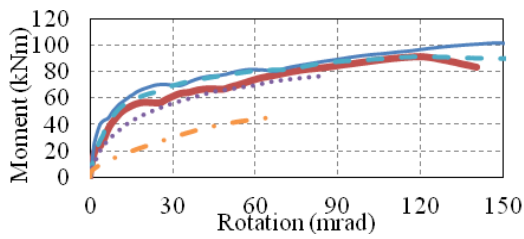
(a) Connection H1 Compression (left) and tension (right)



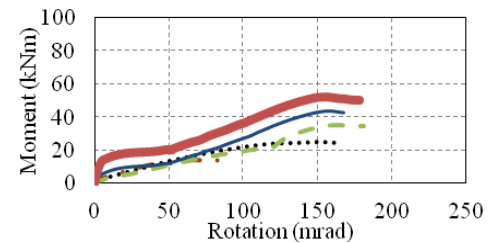
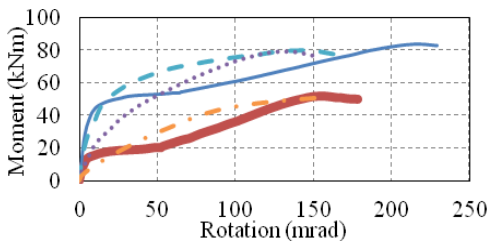
(b) Connection H2 Compression (left) and tension (right)



(c) Connection H3 Compression (left) and tension (right)



(d) Connection H4 Compression (left) and tension (right)



(e) Connection R1 Compression (left) and tension (right)

Fig. 5 Continued

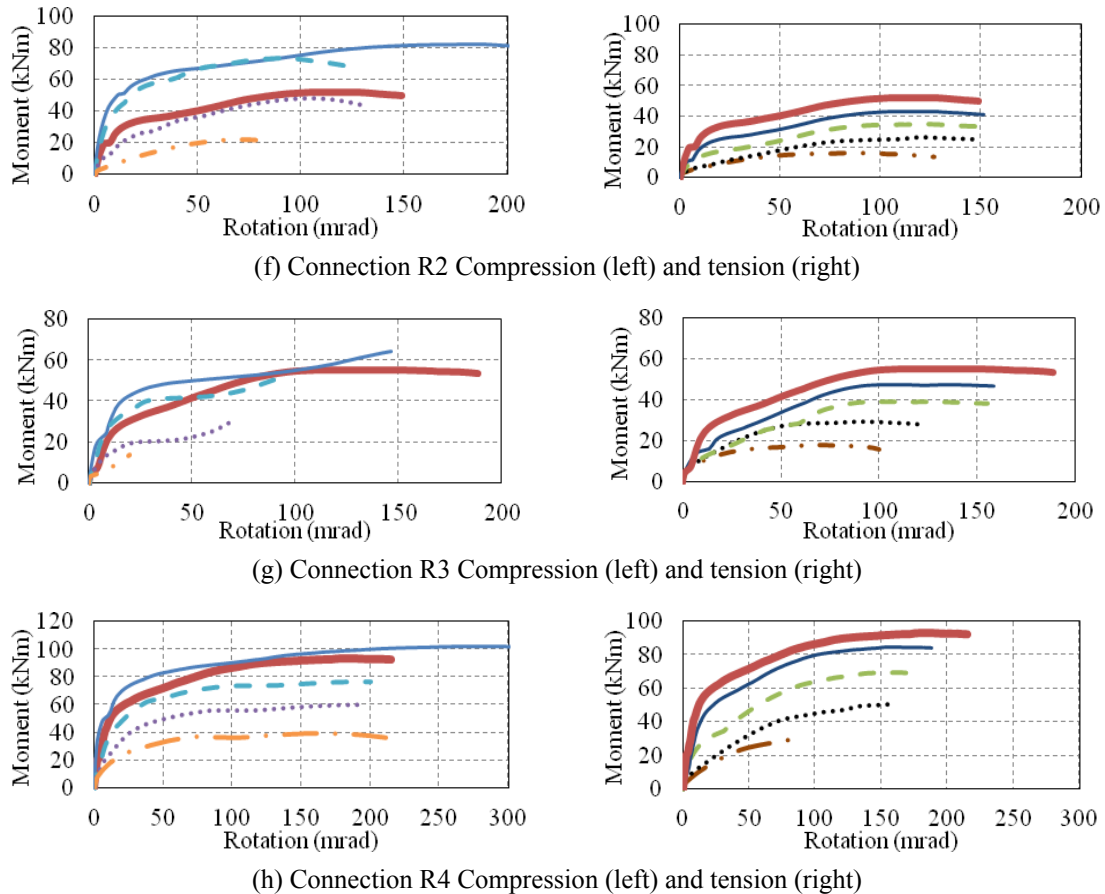


Fig. 5 Moment-rotation relationships for different levels of axial action

($M_y/M_{y,0}$) and the corresponding axial forces ($N/N_{y,t}$ or $N/N_{y,c}$) for the eight connection configurations under study. Tension is represented in Fig. 4 by positive values of the axial force ratio ($N/N_{y,t}$), while compression forces have negative values of $N/N_{y,c}$. It is observed from Fig. 4 that the yield moment capacity ratio ($M_y/M_{y,0}$) decreases as the applied tension force increases due to the shift of the centre of rotation towards the lower tension zone along the height of the joint (i.e., towards the bottom in the case of hogging moments). Conversely, when compression forces are applied, the yield moment ratio ($M_y/M_{y,0}$) reaches its maximum value for compression levels ranging from 20 to 60% of $N_{y,c}$. Importantly, the largest relative increments in maximum yield moment ratios ($M_y/M_{y,0}$) are observed for Connections H1 and R1 (e.g., H1 achieves a yield moment of about 3.7 $M_{y,0}$ when a compression load of 57% of its yield resistance is applied). In contrast, more modest maximum yield capacity enhancements (in the order of 20%) are obtained for Connections R4 and H4 with these maxima occurring at lower levels of compression action (i.e., $N = 0.2 N_{y,c}$ to $0.4 N_{y,c}$). Similarly, the maximum yield moment ratio for Connections H1 and R1 (with gauge distance $d = 65$ mm) is about two times larger than that for Connections H2 and R2 which have stiffer angle details (i.e., gauge distance $d = 40$ mm). These larger relative enhancements due to

compression loads in connections with lower yield strengths (as opposed to stiffer connections with higher strengths) suggest an absolute limit on the yield capacity increase brought about by the application of compression forces through the shift of the centre of rotation. This limit can be related to the absolute difference between tension and compression capacities of the joint. For Connections H1 and R1, the compression capacity (which is governed by the column face in compression) is 8 times higher than their corresponding tension capacity (which is determined by the top angles in bending), whereas for connections R4 and H4, the tension capacity is close to their compression capacity. The maximum bending capacity is obtained when the components dominating the connection compression and tension capacity attain their resistance at similar levels of applied compression force.

Further illustration of the effects of axial action on the bending response at yield is depicted in Fig. 5 which presents the moment-rotation curves for all connections at different levels of axial action. It can be observed from Fig. 5 that for Connections H1, H2, R1 and R2, compressive forces equal or greater than about $0.60 N_{u,c}$ cause noticeable reductions in both the rotational stiffness and yield capacity of the connection due to yielding of the column and reverse channel face components. The same reduction levels are observed for compressive forces equal or greater than $0.40 N_{u,c}$ in Connections H3, H4, R3 and R4. More importantly, in line with the previous discussion, a maximum absolute enhancement of around + 30 kNm (i.e., difference between pure bending yield capacity and maximum bending yield capacity under concurrent compression action) is observed for Connections H1, H2, H3, R1, R2 and R3 regardless of the level of applied compression forces. On the other hand, top, seat and web angle details (Connections H4 and R4 in Fig. 5) exhibit a smaller maximum absolute yield strength enhancement of only + 15 kNm or less which can be attributed to the level of engagement of the column/reverse channel face component already present in Connections H4 and R4 under pure bending. Finally, it can also be observed from Fig. 5 that in all cases when the connection is subjected to both tension and bending, the flexural yield capacity decreases in proportion to the increase in the applied tension force.

3.2.2 Maximum moment

The influence of the applied axial force on the connection maximum moment capacity can be appreciated from Fig. 6 which presents the normalized peak moment-axial interaction curves. The maximum moment capacity is defined herein as the peak moment values immediately before the occurrence of any strength degradation in the moment-rotation relationships of Fig. 5. It can be observed from Fig. 6 that the application of higher tensile forces results in proportionally lower values of maximum moment, which is consistent with the response observed for yield strengths in the previous section. Similarly, a modest compression force leads to an enhancement in the peak moment capacity. The maximum bending capacity ratio ($M_u/M_{u,0}$) is about 1.7, 2.0, 1.9 and 1.6 for Connections H1, H2, R1 and R2, respectively, and between 1.1 and 1.3 for Connections H3, H4, R3 and R4. These differences may be attributed to the plastic mechanisms formed in Connections H1, H2, R1 and R2 which are governed by the bending deformation on the angles in tension. Such plastic mechanisms are inherently more sensitive to the capacity enhancements brought about by the shift of the centre of rotation towards the mid-height of the joint induced by the application of compressive forces. On the other hand, due to the stiffer angle components employed in Connections H3 and R3 and the presence of web angles in Connections H4 and R4, the development of plasticity in these connections entails a stronger engagement of the column/channel faces which have smaller deformation capacities and therefore develop smaller relative enhancements in their peak bending capacity.

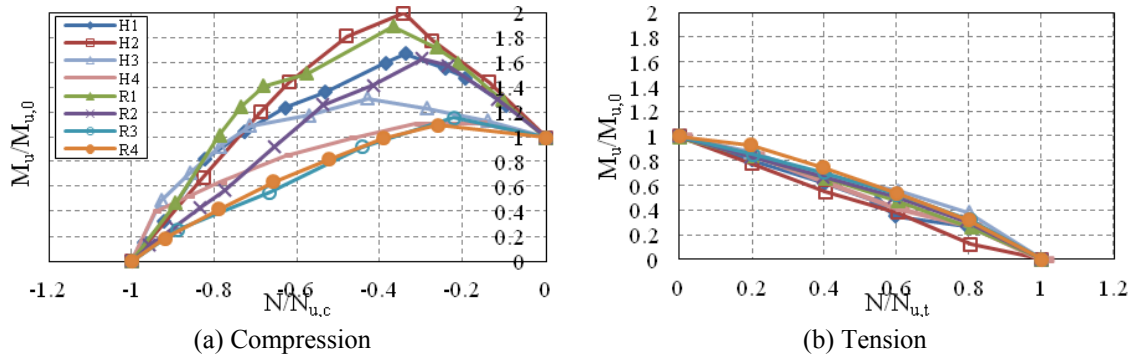


Fig. 6 Moment-axial interaction curves at ultimate

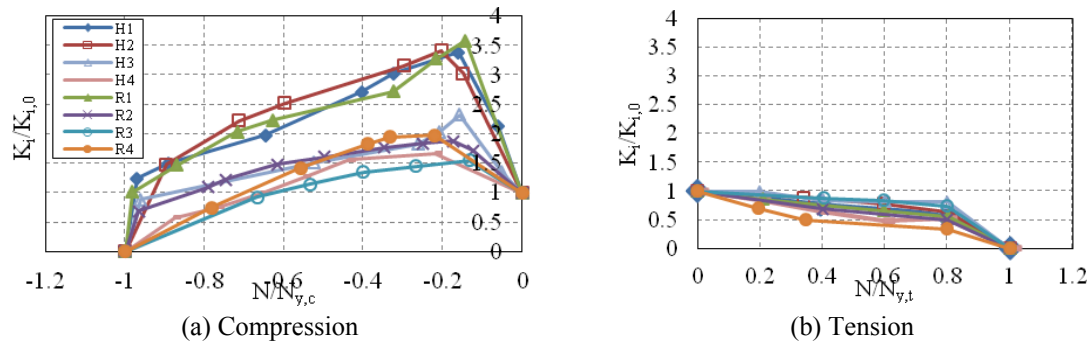


Fig. 7 Initial rotational stiffness for different levels of axial force

The above observations can be corroborated with reference to Fig. 5. It can be noted from Fig. 5 that when the connection is subjected to both tension and bending, the maximum flexural capacity decreases in proportion to the increase of the applied tension force. However, the effects of the imposed compression force on the connection maximum response is more involved. Importantly, the moment-rotation relationship in the post-yield stage for $N = 0$, $N = 20\% N_{u,c}$ and $N = 40\% N_{u,c}$ follow similar trends. However, the connection bending capacity ratio ($M_u/M_{u,0}$) decreases with the increasing imposed compression force for $N \geq 40\% N_{u,c}$ due to local buckling of the column face in compression.

3.2.3 Rotational stiffness

Fig. 7 illustrates the influence of the axial force on the rotational stiffness (K_i) of the eight connections considered in this study normalized by the corresponding rotational stiffness under pure bending ($K_{i,0}$). The rotational stiffness was determined from the bi-linear idealization of the moment-rotation curves. It can be appreciated from Fig. 7 that increasing levels of tension force cause proportional reductions in the joint rotational stiffness whereas modest compression forces lead to an increase in the relative stiffness. This is consistent with the previously presented results for yield capacities. It is evident from Fig. 7 that for tension forces of up to 80% of $N_{y,t}$, the relative rotational stiffness is reduced by up to 50% on average whereas a steep reduction in stiffness can be observed for tension forces greater than 80% of $N_{y,t}$. Also, when the imposed compression force

ratio ($N/N_{y,c}$) is between 15% and 20%, the initial rotational stiffness ratio ($K_i/K_{i,0}$) of the connections reaches its maximum value.

3.2.4 Rotation capacity

The influence of the axial force on the connection rotation capacity is presented in Fig. 8 where ultimate rotations (R_u) are normalised with respect to the rotation capacity under no axial action ($R_{u,0}$). The ultimate rotations are defined as those corresponding to an 80% decrease in the maximum rotational strength of the connection. It can be observed from Fig. 8 that when the applied tension force is less than about 50% of $N_{u,t}$, the ultimate rotation values are largely within $\pm 20\%$ of the corresponding ultimate rotation under pure bending. However, for larger tension forces ($N/N_{u,t} > 50\%$), more significant reductions in the rotation capacity can be observed. On the other hand, when the applied compression force is less than 50% of $N_{u,c}$, the rotation capacity ratio is larger than 1 in all cases except R3. In the case of Connection R3, the maximum value of $R_u/R_{u,0}$ is only 1.2 when 20% of the failure compression load is applied simultaneously with the flexural demands on the connection. It is also important to note, with reference to the moment-rotation relationships presented in Fig. 5, that the absolute ultimate rotation values observed are greater than 60 mrad in all cases (except for Connection R3 subjected to combined bending and significant compression). Importantly, ultimate rotations in excess of 120 mrad are observed when the axial forces are limited to 80% of their corresponding tension or compression resistance. The limited rotational capacity of Connection R3 under compression is attributed to the inherently less ductile failure mechanism developed in this detail which concentrates most of the plastic deformations within a relatively thin channel face.

3.3 Combined bending and shear loads

In order to assess the influence of shear forces on the moment-rotation behaviour of bolted angle connections, the interaction relationships between moment capacities and the applied shear forces are examined in this section with reference to Figs. 9-12. It should be noted that in these figures, positive shear forces are assumed to act from top to bottom whereas hogging and sagging moments are assigned positive and negative values, respectively. In all cases, the connections were subjected to initially prescribed shear forces followed by the application of increasing moment

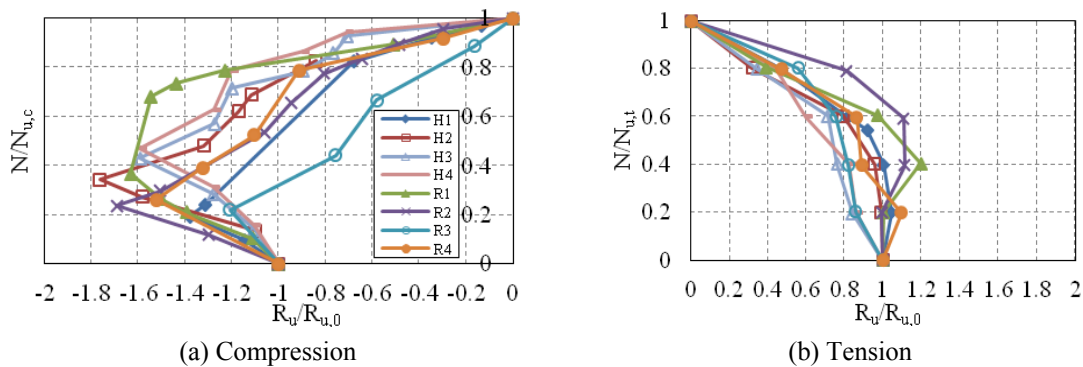


Fig. 8 Rotation at ultimate for different levels of axial force

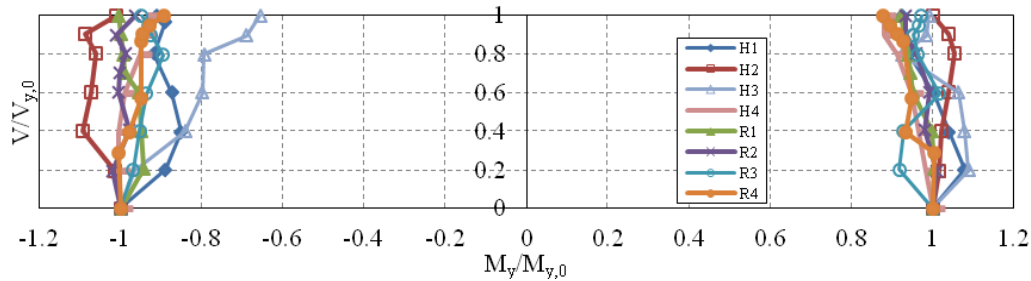


Fig. 9 Shear-moment interaction curves at yield

actions. As before, yield points are determined from bi-linear idealizations while maximum values correspond to peak levels of imposed loads.

3.3.1 Yield moment

Fig. 9 presents the shear-moment interaction curves at yield for the eight connections under consideration. It can be concluded from Fig. 9 that the shear force has a negligible influence on the connection yield moment capacity for virtually all the cases examined herein. The moment ratio at yield ($M_y/M_{y,0}$) does not typically vary by more than $\pm 10\%$. The exception is H3 for which $M_y/M_{y,0}$ becomes less than 0.8 for shear forces larger than 80% of its corresponding yield shear capacity ($V/V_{y,0}$); this can be attributed to the significant rotation in the angle induced by the extreme case represented by the inherent rotational flexibility of Holo-bolts in the combination of thick angles with a thin column face which reduces the overall connection bending capacity.

The above discussion is further illustrated with reference to Fig. 10 which presents a comparison of the connection moment-rotation relationships for hogging moments under different shear load levels. It can be observed from Fig. 10 that the imposed shear forces largely have an insignificant influence on both the connection rotational stiffness and yield moment.

3.3.2 Maximum moment

Fig. 11 presents the shear versus maximum moment interaction curves for the connections under consideration. It is evident from the figure that for hogging moments (positive values), shear forces larger than 60% of the ultimate shear resistance ($V_{u,0}$) are accompanied by a reduction of more than 20% in the ultimate moment capacity ($M_{u,0}$) for Connections H1, H3, H4, R3 and R4. Conversely, significant levels of ultimate bending resistance are maintained in connections H2, R1 and R2 up to the simultaneous application of over 90% of their corresponding shear capacity ($V_{u,0}$). Similar trends are observed for the connection response under combined shear and sagging (negative) moments, with the exception of the extreme geometric case of Connection H3 for which more significant reductions in moment capacity occur for shear loads as low as 30% of $V_{u,0}$. The above observations can be examined further by assessing the hogging moment-rotation curves at different levels of shear loads as depicted in Fig. 10. As shown in the figure, shear forces lower than $0.6 V_{u,c}$ have positive effects on the maximum moments for Connections H2, H3 and H4 where an absolute increment of around + 10 kNm is observed. On the other hand, when shear loads greater than $0.6 V_{u,c}$ are applied, notable reductions in the maximum moment are evident especially for Connections H3, H4 and R4.

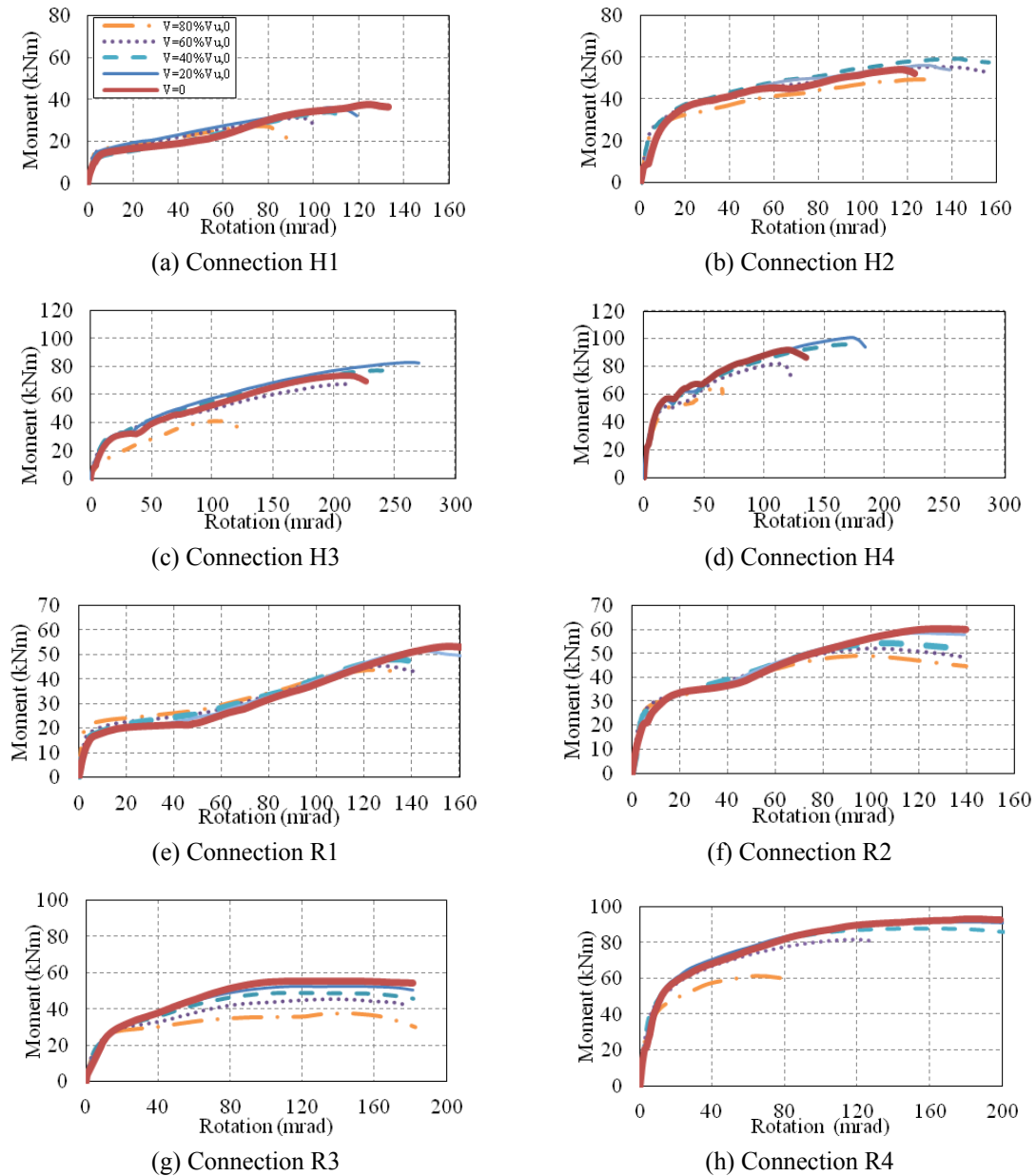


Fig. 10 Influence of shear force on the connection moment-rotation relationships

3.3.3 Rotational stiffness and capacity

Fig. 12 depicts the normalized connection rotation capacity at different levels of shear force. It can be noted from this figure that for sagging moments (negative values), shear forces lower than around 60% of the ultimate shear resistance ($V_{u,0}$) result in an increase of more than 40% in the ultimate rotational capacity ($R_{u,0}$) for Connections H1, R1 and R2. Conversely, shear forces lower

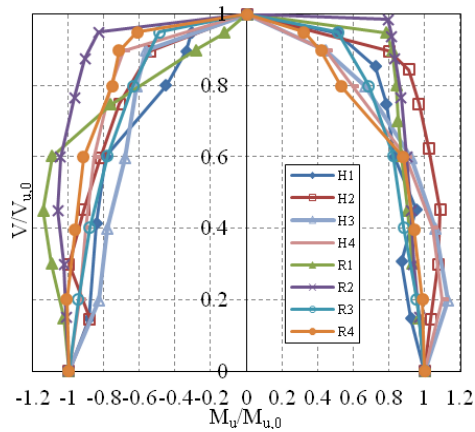


Fig. 11 Shear-moment interaction curves at ultimate

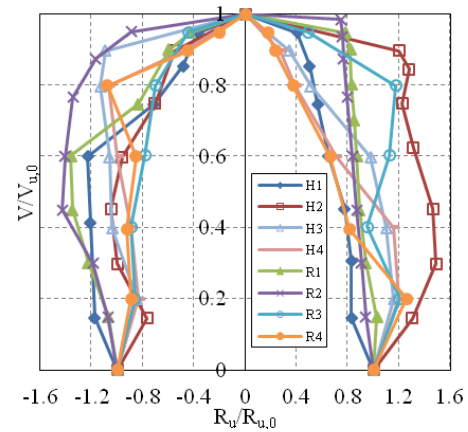


Fig. 12 Rotation at ultimate for different levels of shear force

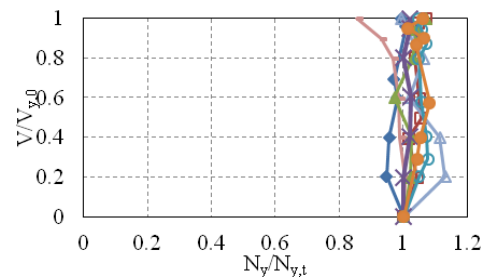
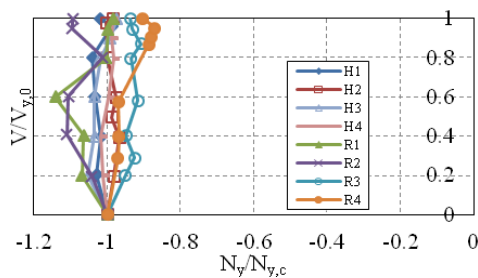


Fig. 13 Shear-axial load interaction curves at yield. Compression (left) and tension (right)

than 60% of $V_{u,0}$ cause a 20% reduction in the ultimate rotation for Connection H4, R3 and R4. Similar trends are observed for the connection response under combined shear and hogging moments.

The effect of the shear force on the connection initial rotational stiffness and rotation capacity can be discussed further with reference to Fig. 10. It can be observed from the figure that the initial rotational stiffness as well as the connection yield capacity remains relatively unaltered regardless of the level of concurrent shear action applied. In the case of Connections H1 and R1, increasing levels of shear force result in proportional reductions in the overall connection ductility. For example, the rotation capacity of Connection H1 reduces from over 120 mrad (when no shear action is applied) to less than 90 mrad (when a shear force of 0.8 $V_{u,0}$ is applied). On the other hand, the application of shear loads lower than 40% of the connection ultimate shear capacity result in slight variations in the rotation capacity for Connections H2, H3, H4, R3 and R4. However, it is important to note that, regardless of the level of concurrent shear action, the absolute maximum rotations in all cases are in the order of 80 mrad or higher.

3.4 Combined axial and shear loads

3.4.1 Axial yield capacity

Fig. 13 depicts the interaction curves for combined axial and shear actions at yield. As shown

in the figure, the influence of shear on axial capacity is largely limited to within $\pm 10\%$ for most cases. Similarly, Fig. 14 presents the connection tension-displacement relationships under different levels of applied shear load. It is evident from Fig. 14 that the effect of the shear force on the connection tensile stiffness and tensile yield capacity is negligible with relatively minor influence on the tension capacity for Connection H1, H2, H3, R1, R2 and R3.

3.4.2 Maximum axial capacity

The influence of shear on the ultimate axial capacity is comparatively more significant than on the yield forces, as illustrated in Fig. 15, particularly for $V/V_{u,0}$ ratios greater than 0.6 and especially for Connections H4 and R4. In the case of combined tension and shear (Fig. 15(b)), an increase of up to 20% in the tension capacity is induced by the imposed shear load for Connections H1, H2, R1, R2 and R3 when $V/V_{u,0}$ is less than 0.9. On the other hand, a reduction of around 20%

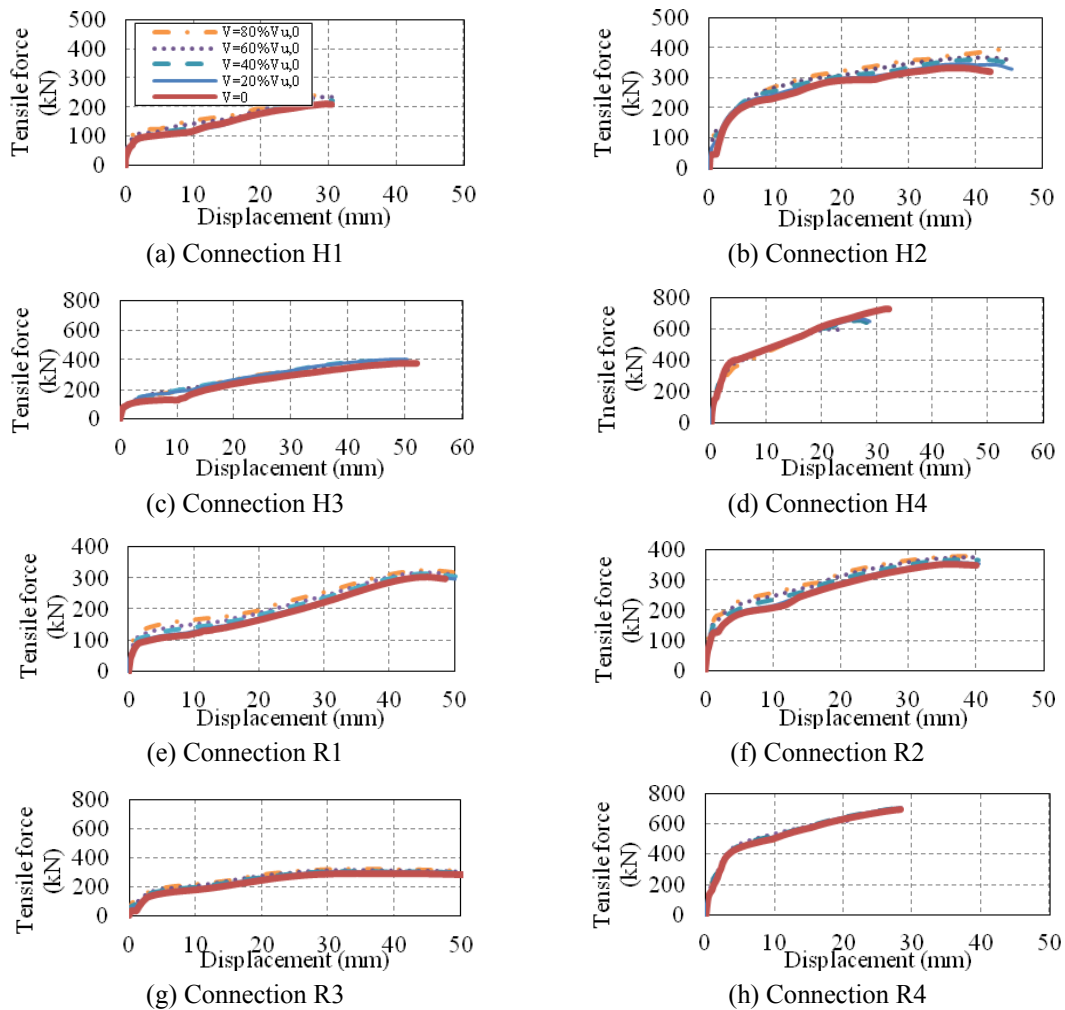


Fig. 14 Influence of shear force on the connection tension-displacement relationships

in the tension resistance occurs in Connections H4 and R4 for shear loads less than 60% of its ultimate shear resistance ($V_{u,0}$) whereas a more notable decrease of the tension capacity occurs when the shear load is larger than 60% of $V_{u,0}$. This can be attributed to the large absolute values of shear increments required to achieve similar relative shear increments in top, seat and web angle connections as compared with top and seat angle connections which have smaller $V_{u,0}$ capacities. Also, the reduction of the relative tension resistance of Connection H3 becomes significant for shear loads greater than 80% of $V_{u,0}$. This can be attributed to the unfavourable detail of Connection H3 which includes a stiff thick angle that concentrates stresses on the Holo-bolt causing extensive yielding of its shank and its subsequent pull-out. These effects can be corroborated from Fig. 14 where significant reductions in ductility are evident for Connection H3.

3.4.3 Axial ductility

The effect of shear forces on the connection ultimate tensile and compression deformation is presented in Fig. 16. The ultimate tensile and compression displacements are defined as those corresponding to a 20% decrease in the maximum rotational strength of the connection. It can be observed from Fig. 16(a) that the applied shear forces improve the ultimate compression displacement by 20% for the cases of Connections H3 and R3. However, for larger shear forces

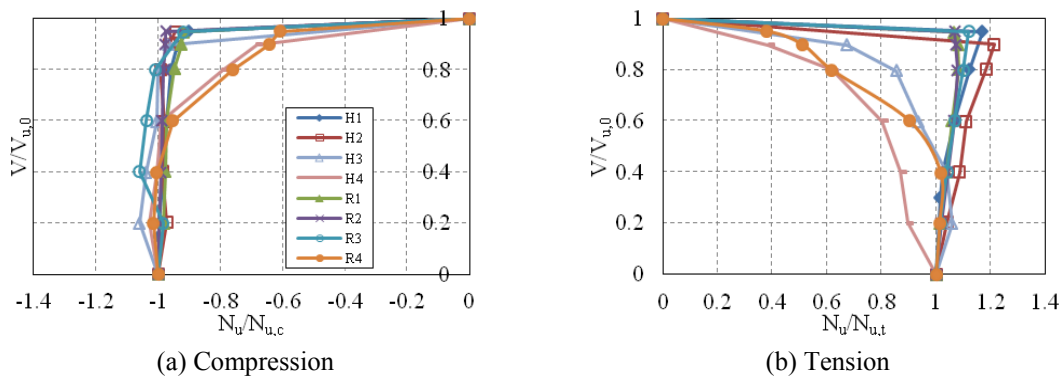


Fig. 15 Shear-axial load interaction curves at ultimate

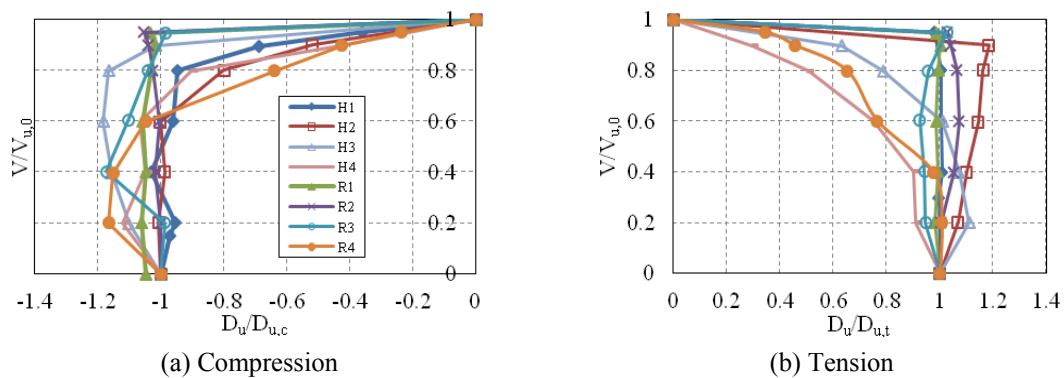


Fig. 16 Axial displacement at ultimate for different levels of shear force

($V/V_{u,0} > 60\%$), significant reductions in the compression ductility can be observed, especially for Connections H1, H4 and R4. Similarly, as illustrated in Fig. 16(b), when the applied shear force is less than about 60% of the peak shear force, the ultimate tensile displacements are largely within $\pm 20\%$ of the maximum tensile displacement under pure tensile loads.

4. Simplified modelling

4.1 Component-based representation

The detailed numerical model discussed above can faithfully capture the complex behavioural interactions that occur in different connection details subjected to various load combinations. Nonetheless, such models are computationally demanding and not suited for conventional design calculations. For this purpose, it is often more effective to use component based mechanical representations of the connections. This section describes a component-based model assembled in order to examine the response of semi-rigid open beam-to-tubular column angle connections under various loading conditions. In line with the component-based approach, the model outlined in Fig. 17 consists of two rigid bars, representing the column centreline and the beam end, connected through a series of nonlinear springs at each bolt-row level. The following connection components have been considered in assembling the response of the bolted angle connections:

- (1) Bolts in tension (F_{bt}, K_{bt})
- (2) Bolts in shear (F_{bs}, K_{bs})
- (3) Column/channel face in bending (F_{cft}, K_{cft})
- (4) Angle in bending (F_{at}, K_{at})
- (5) Column/channel face in compression (F_{cfc}, K_{cfc})
- (6) Angle leg in compression (F_{ac}, K_{ac})
- (7) Angle leg in bearing (F_{ab}, K_{ab})
- (8) Beam flange in bearing (F_{bfb}, K_{bfb})
- (9) Beam web in bearing (F_{bwb}, K_{bwb})

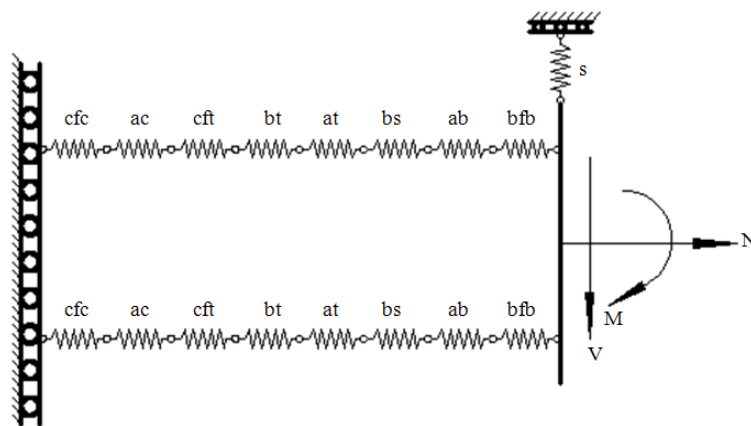


Fig. 17 Simplified spring model for angle connections under combined axial, shear and bending actions

Table 3 Component characteristics *

Component	Stiffness	Capacity
Bolts in tension	Standard bolt (CEN 2005): $K_{st} = 1.6 \frac{EA_s}{L_b}$	Standard bolt (CEN 2005): $F_{st} = f_{u,b} A_s$
	Hollo-bolt (Elghazouli <i>et al.</i> 2009): $K_{ht} = \begin{cases} 195 \text{ kN/mm} \\ 160 \text{ kN/mm} \end{cases}$	Hollo-bolt (Elghazouli <i>et al.</i> 2009): (Elghazouli <i>et al.</i> 2009) $F_{ht} = \begin{cases} 78 \text{ kN} \\ 32 \text{ kN} \end{cases}$
Bolts in shear	Standard bolt (CEN 2005): $K_{ss} = 16 \frac{d_b^2 f_{u,b}}{d_{M16}}$	Standard bolt (CEN 2005): $F_{ss} = \frac{A_s f_{u,b}}{\sqrt{3}}$
	Hollo-bolt (Liu <i>et al.</i> 2012b): $K_{ht} = \begin{cases} 92 \text{ kN/mm} \\ 74 \text{ kN/mm} \end{cases}$	Hollo-bolt (Liu <i>et al.</i> 2012b): $F_{ht} = \frac{A_s f_{u,b} + A_{s,h} f_{u,h}}{\sqrt{3}}$
Column/ channel face in bending	(Elghazouli <i>et al.</i> 2009) $K_{cft} = \frac{\pi E t_c^3}{6(1-\nu^2) C_t \left(\frac{b_c - t_c}{2}\right)^2}$ with $C_t = Q_t (0.24 e^{-0.3t/m_c})$ where (Liu <i>et al.</i> 2012a) $Q_t = \begin{cases} 6 L^{-0.4} & \text{if } L < 100 \text{ mm} \\ 1 & \text{if } L \geq 100 \text{ mm} \end{cases}$ and $m_c = (b_c - 2t_c - 2r_c)/2$	Channel face (Málaga-Chuquitaype 2011): $F_{cft} = f_{y,c} t_c^2 \left(\frac{2R_m - d_0}{2R_m - d_{bh}} \right) \left[\frac{\pi}{d_0 - 2R_m} \frac{d_0 - R_m}{2} + 2 \frac{i + 2c + d_0}{2R_m - d_0} \right]$ with $R_m = (b_c - t_c - i)/2$ Column face (Gomes 1996): $F_{cft} = \min(F_{cft,1}, F_{cft,2})$ with $F_{cft} = \delta \varepsilon \frac{t_c^2 f_{y,c}}{4}$, $F_{cft,2} = \begin{cases} \frac{n_b \pi d_0 t_c f_{y,c}}{\sqrt{3}} & \text{if } 2(i + 0.9d_0) > n_b \\ \frac{2(i + 0.9d_0) t_c f_{y,c}}{\sqrt{3}} & \text{if } 2(i + 0.9d_0) < n_b \end{cases}$
	(Málaga-Chuquitaype and Elghazouli 2010b): $K_{at} = \frac{E b_{eff} t_a^3}{d'^3}$ with $d' = d - 0.8r_a - t_a - (1 - f_{pry}) \frac{d_b}{2}$	(Málaga-Chuquitaype and Elghazouli 2010b): $F_{at} = \min \left(\frac{4M_{pl}}{d'}, \frac{2M_{pl} + c' \sum F_{bt}}{d' + c'} \right)$ where $M_{pl} = 0.25 b_{eff} t_a^2 f_{y,a}$, $c' = c + (1 - f_{pry}) \frac{d_b}{2}$

Table 3 Continued

Column/ channel face in Compression	$K_{cft} = \frac{\pi E t_c^3}{6(1-\nu^2)C_c \left(\frac{b_c - t_c}{2}\right)^2}$ (Elghazouli <i>et al.</i> 2009) where (Liu <i>et al.</i> 2012a): $C_c = Q_c \cdot (0.3 \ln(C/B) + 0.03)$ $Q_c = \begin{cases} 7 L_c^{-0.4} & \text{if } L_c < 100 \text{ mm} \\ 1 & \text{if } L_c \geq 100 \text{ mm} \end{cases}$	With thin angle (Liu <i>et al.</i> 2012a): $F_{cfc,1} = 2 \cdot f_{y,c} t_c^2 \left[\sqrt{\frac{C+3B}{C-B}} + \sqrt{\frac{2B}{C-B}} + \frac{h}{c} \right],$ and $C = b_c - t_c$ $B = \begin{cases} \min(b_a; b_b) & \text{if } b_c \leq \min(b_a; b_b) \\ b_c - 2t_c - 2r_c & \text{if } b_c > \min(b_a; b_b) \end{cases}$
Angle leg in compression	(CEN 2005): $K_{ac} = \frac{n'_b E d_0 t_a}{a}$	With thick angle (Liu <i>et al.</i> 2012a): $F_{cfc,2} = 2 \cdot f_{y,c} t_c^2 \left[\frac{2L_c}{C-B} + \sqrt{2} \frac{B}{C} + \frac{h}{c} \right]$ (Liu <i>et al.</i> 2012a): $F_{ac} = \begin{cases} 0.5 \cdot f_{y,a} t_a^2 \left[\frac{B}{L_A} \cdot \left(1 + \frac{L_a}{A}\right) \right] & \text{if } A \leq L \\ 1.5 \cdot f_{y,a} t_a^2 \left[\frac{B}{A} \right] & \text{if } A > L \end{cases}$ with $A = \frac{\sqrt{(C+3B) \cdot (C-B)}}{2}$
Plate in bearing	$K_b = 24 k_b k_a d_b f_{u,p}$ (CEN 2005)	$F_{pb} = n_b 2.5 a f_{u,p} d_b t_p$ with $\alpha = \min\left(\frac{e_b}{3d_0}; \frac{e_b}{3d_0} - \frac{1}{4}; \frac{f_{u,b}}{f_{u,p}}; 1\right)$ (CEN 2005)

* The definition of variables and notations employed can be found in Appendix A

The expressions used for the estimation of the stiffness and capacity of individual components are summarized in Table 3 while details of the assemblage of the joint response subjected to pure loads are presented in Table 4. The stiffness and capacity of Holo-bolts in tension and shear are based on previous experimental results (Elghazouli *et al.* 2009, Liu *et al.* 2012b) while the resistance of the column/channel face and the angle under compression and tension are derived from their corresponding yield mechanisms (Liu *et al.* 2012b). The mechanical characteristics of other components can be determined from relationships proposed by other researchers (Gomes 1996, Pucinotti 2001, Málaga-Chuquitaype and Elghazouli 2010a, b, Liu *et al.* 2012a, b). Also, after yielding, a strain hardening coefficient in the range of 1% - 5% is employed to define the post-elastic stiffness, in line with typical values found by other investigators (Faella *et al.* 2000).

In order to incorporate shear effects within simplified component representations, the full connection shear force-vertical deformation behaviour is represented by a single spring (indicated as 's' in Fig. 17). Besides, an elastic-perfectly plastic model for the shear force-displacement response of this shear spring is considered. Both of these assumptions are justified in light of the results presented in the previous section in which the bending response of angle connections to tubes was observed to be largely unaffected by the simultaneous application of shear actions within the ranges of typical design scenarios. The component-based model depicted in Fig. 17 was

Table 4 Assemblage of the joint response under single loads*

Loads	Stiffness	Capacity
Tension	$K_t = \sum_{i=1}^{n_r} K_{it}$ <p>with $K_{it} = \frac{1}{\frac{1}{K_{cft}} + \frac{1}{K_{at}} + \frac{1}{K_{bt}} + \frac{1}{K_{bs}} + \frac{1}{K_{ab}} + \frac{1}{K_{bb}}}$</p> <p>where K_{it} is the tensile stiffness of the i-th bolt row, n_r is the number of the bolt rows in tension.</p>	$F_t = \sum_{i=1}^{n_r} F_{it}$ <p>with</p> $F_{it} = \min(F_{cft}; F_{at}; F_{bt}; F_{bs}; F_{ab}; F_{bb})$ <p>Where F_{it} is the tensile resistance of the i-th bolt row.</p>
Compression	$K_c = \frac{2}{\frac{1}{K_{cfc}} + \frac{1}{K_{ac}} + \frac{1}{K_{bs}}}$	<p>Blind-bolted angle configuration (Liu <i>et al.</i> 2012a): $F_c = F_{cfc,1} + F_{ac}$</p> <hr/> <p>Combined angle/channel configuration (Liu <i>et al.</i> 2012a): $F_c = \min[(F_{cfc,1} + F_{ac}); (F_{cfc,2})]$</p>
Bending	<p>Top and seat angle connections:</p> $K_b = y_t^2 / K_t$ <p>where K_t is the stiffness of the top angle bolt-row and y_t is the distance between the top angle bolt-row and the horizontal of the bottom angle (Málaga-Chuquitaype and Elghazouli 2010b).</p> <hr/> <p>When web angles are included:</p> $K_M = y_{eq}^2 \left(\frac{1}{K_{cft}} + \frac{1}{K_{eq}} \right)$ $K_{eq} = \sum K_i y_i / y_{eq}, \quad y_{eq} = \sum K_i y_i^2 / \sum K_i y_i$ <p>where K_i is the stiffness of the i-th bolt-row, and y_i defines the location of the bolt-row with reference to the assumed point of rotation (Pucinotti 2001).</p>	$M = \left(\begin{array}{c} 1.11 + 0.1 \frac{d'}{t_f} \\ -0.02 \frac{b_c}{t_c} \end{array} \right) \frac{2M_{pl}}{d'} H$ $+ \sum_j^{n-1} F_j y_j$ <p>Where j is the number of remaining bolt-rows and is F_j the axial force in the j-th bolt-row, H is the summation of the beam height (Málaga-Chuquitaype and Elghazouli 2010b).</p>
Shear	<p>Top and seat angles:</p> $K_s = K_{top} + K_{bottom}$ $= \frac{1}{\frac{1}{K_r} + \frac{1}{K_{at}} + \frac{1}{K_{ab}} + \frac{1}{K_{cftb}} + \frac{1}{K_{bs}}} + \frac{1}{\frac{1}{K_{ab}} + \frac{1}{K_{cftb}} + \frac{1}{K_{bs}}}$ <p>with $K_r = \frac{d^2}{a_2} \left(\frac{1}{\frac{1}{K_{cft}} + \frac{1}{K_{bt}}} \right)$ (Liu <i>et al.</i> 2012b)</p>	<p>A conservative approach was employed to define the connection ultimate shear capacity as that corresponding to the summation of capacities of the weakest components within each bolt-row (Liu <i>et al.</i> 2012b):</p>

Table 4 Continued

Shear	<p>Web angles: $K_{web} = \sum_{i=1}^{n_r} \frac{2}{\frac{1}{K_{ab}} + \frac{1}{K_{bs}} + \frac{1}{K_{cfb}}}$</p> <p>with $K_i = \frac{2}{\frac{1}{K_{ab}} + \frac{1}{K_{bs}} + \frac{1}{K_{cfb}}}$</p> <p>where n_r is the number of bolt rows, K_i is the stiffness of the i-th bolt-row in the double web angle (Liu <i>et al.</i> 2012b).</p>	$F_s = \begin{cases} F_{at} + \sum_{bottom} F_{bs} \\ \text{or} \\ \sum_{top} F_{ss} + \sum_{bottom} F_{bs} \end{cases}$
-------	--	--

*The definition of variables and notations employed can be found in Appendix A

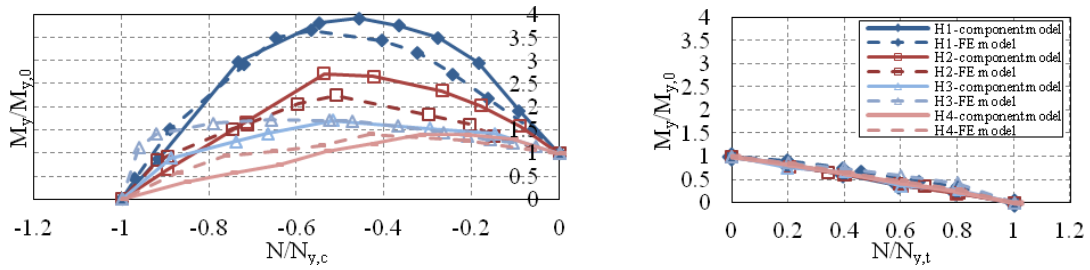
assembled using the FE program ABAQUS V6.7 (2003), but can be similarly employed within any frame analysis representation.

4.2 Comparison with detailed models

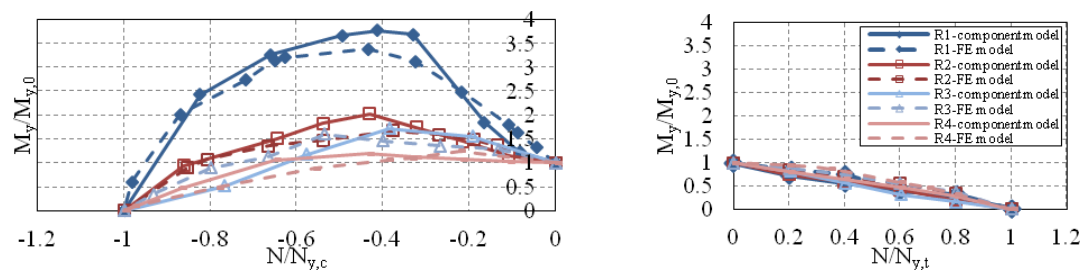
This section compares the interaction relationships between axial and bending response obtained from the component-based model with the results provided by means of the detailed numerical simulations. These comparisons are summarized in Figs. 18-21 for moment-axial actions at yield and at ultimate, as well as the connection initial rotational stiffness and rotational capacity. As before, the results are normalized with respect to their corresponding resistance when the connections are subjected to pure tension, compression or bending action.

It is evident from Figs. 18 and 19 that the component-based model provides reasonably good agreement of the connection moment-axial interactions with the results of the detailed finite element model, except for some inevitable differences arising from the simplifications and idealisations adopted in the component-based representation. In particular, the discrepancies observed in Fig. 18 for Connection H3 subjected to axial actions in the range of 0.6–1.0 $N/N_{y,c}$ are related to the limitations of the Hollo-bolt axial response idealization. The very stiff angle employed in Connection H3 results in complex local interactions that eventually cause the pulling-out of the Hollo-bolt which is difficult to model within a component-based approach. Also, as depicted in Fig. 19, the moment capacity ratio ($M_u/M_{u,0}$) obtained by means of the spring models is slightly underestimated (within a range of $\pm 10\%$) for H2, H4, R1 and R4 compared with the numerical results. This can be attributed to the conservative estimate of the ultimate compression capacity $M_{u,0}$ under pure compression load (Liu *et al.* 2012a).

Similarly, the comparisons of the effect of axial actions on the connection initial rotational stiffness and rotational capacity as obtained from the FE model, and those predicted by means of the proposed spring representations, are presented in Figs. 20 and 21, respectively. It can be noted from Fig. 20 that good estimates for the connection initial rotational stiffness ratio ($K_i/K_{i,0}$) under different level of axial loads are obtained in all cases. A difference of around 15% between the component-based estimations and the numerical simulations is observed for Connections H1 and R1 when they are subjected to tension forces exceeding 80% of their yield tension capacity. Also, it is shown in Fig. 21 that the component-based model provides a reasonably good prediction of the connection rotation capacity under different levels of axial force. Some discrepancies observed in Fig. 21 are related to the approximation of the post-elastic stiffness with a constant strain

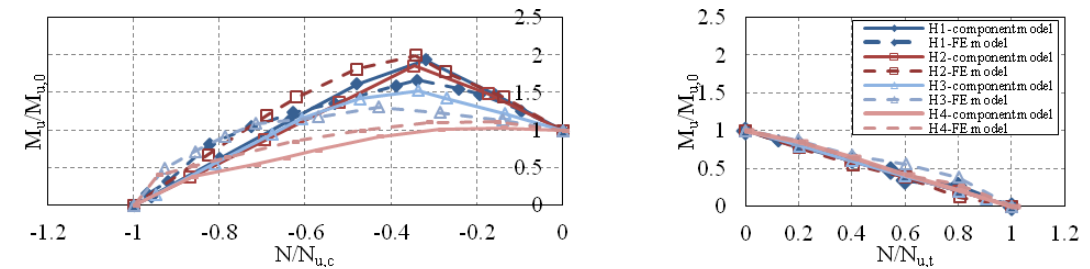


(a) Hollo-bolted angle connections compression (left) and tension (right)

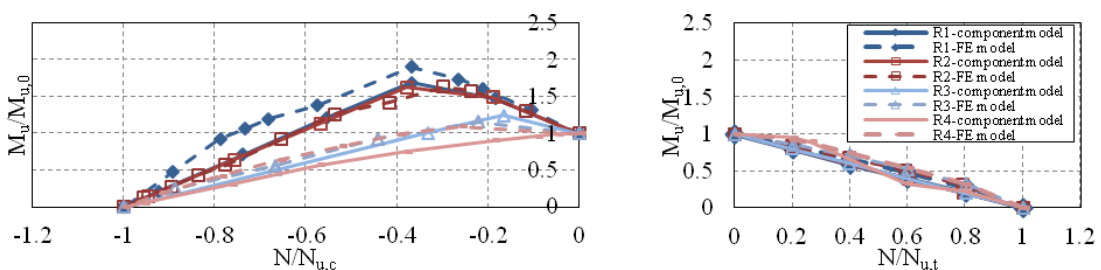


(b) Combined channel/angle connections compression (left) and tension (right)

Fig. 18 Comparison of moment-axial interaction curves at yield

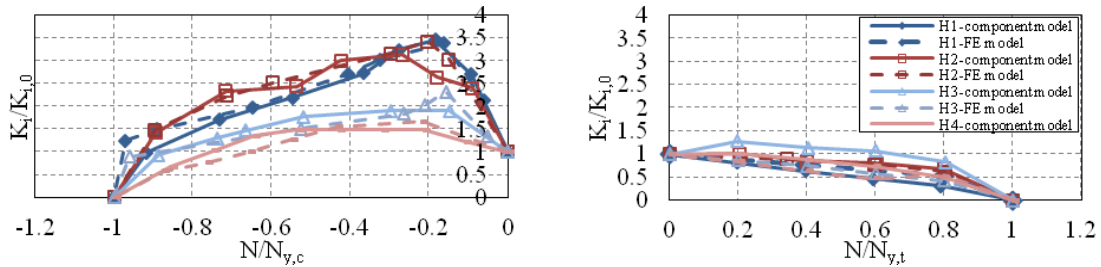


(a) Hollo-bolted angle connections compression (left) and tension (right)

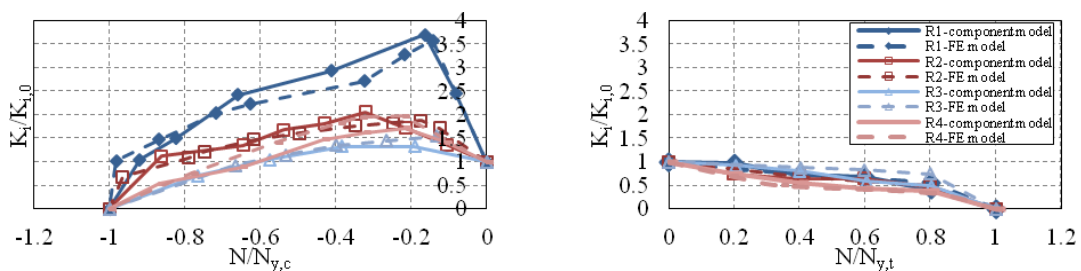


(b) Combined channel/angle connections compression (left) and tension (right)

Fig. 19 Comparison of moment-axial interaction curves at ultimate

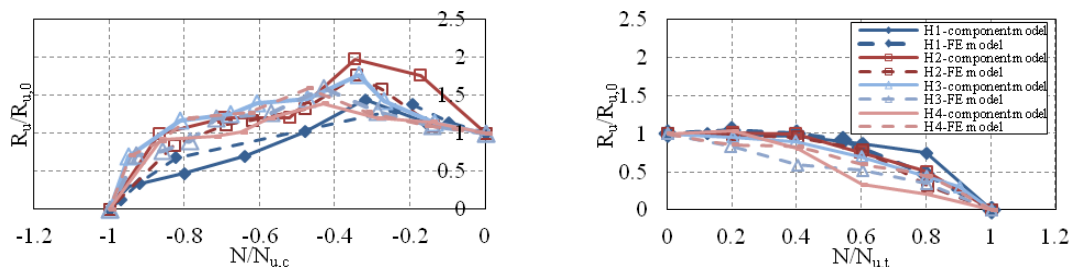


(a) Hollo-bolted angle connections compression (left) and tension (right)

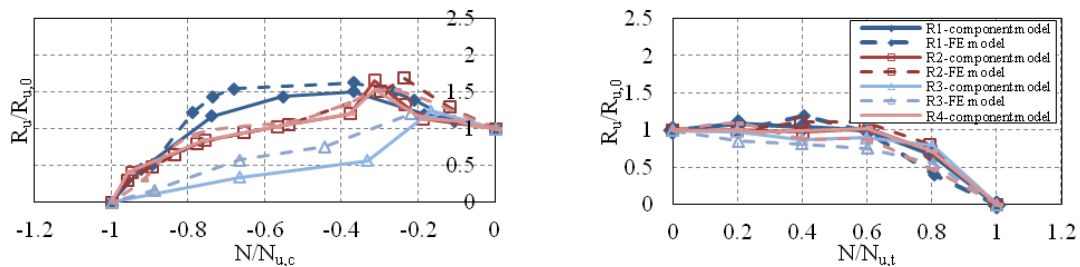


(b) Combined channel/angle connections compression (left) and tension (right)

Fig. 20 Comparison of connection initial rotational stiffness at different axial loads



(a) Hollo-bolted angle connections compression (left) and tension (right)



(b) Combined channel/angle connections compression (left) and tension (right)

Fig. 21 Comparison of connection rotational capacity at different axial loads

hardening coefficient in the range of 1%-5% for each component.

Overall, the connection moment-rotation response at the pre-yielding and post yielding phases under different level of axial actions are closely represented by the component-based model as compared with the FE simulations. This good correlation with the numerical simulations shows that the component-based spring model can be used with a high degree of reliability to capture the response of bolted angle connections under various load combinations.

5. Conclusions

This paper examined the behaviour of two cost-effective and practical connection details subjected to combined loads by means of numerical studies and simplified component-based models. Eight connection details representing a practical range of stiffness and capacity were selected in order to investigate the joint response to combined actions including: (i) bending and axial, (ii) bending and shear, and (iii) axial and shear forces. The main response stages were identified and key behavioural trends were discussed.

The influence of the axial force on the connection bending capacity (at both yield and ultimate), rotational stiffness and rotational capacity was evaluated. It was shown that the application of increasing tensile forces results in corresponding reductions in moment resistance, while a modest compression force leads to enhanced moment capacities. The maximum bending capacity was obtained when the components controlling the connection compression and tension resistance reached their ultimate capacity simultaneously at a given level of compressive force. Moreover, tensile forces decreased the rotational stiffness of the connections whereas concurrent compression forces led to an increase in the relative stiffness. Importantly, the absolute values of ultimate rotation capacity for the range of connections and load combinations analysed in this study remain largely in excess of the requirements imposed by typical design scenarios.

With regards to the influence of shear load on the connection capacity, it was shown that the shear force has a negligible influence on the connection yield moment capacity whereas the effect of the shear force on the connection ultimate moment resistance becomes noticeable only when the applied shear force exceeds 60% of the shear capacity. It was also observed that shear force ratios lower than 80% of $V_{u,0}$ do not have a significant influence on the tension and compression axial capacity. Additionally, ultimate absolute rotations in the order of 80 mrad or higher were found to be maintained regardless of the level of concurrent shear and bending action in most cases.

A component-based spring model was presented and its ability to represent the connection response under combined loads was examined. The results obtained by means of the component-based representation were compared with detailed numerical simulations in order to assess its accuracy in terms of moment-axial force relationships. In general, the component-based estimations were found to correlate very well with the numerical results. The close correlation with the numerical simulations shows that the component-based spring model can be reliably used to capture the response of bolted angle connections.

Acknowledgments

The support of Tata Steel Tubes for the research described in this paper is gratefully acknowledged. Additionally, the first author would like to acknowledge the grant provided by The

China Scholarship Council and The UK Department for Innovation, Universities & Skills for her doctoral research studies at Imperial College London through a UK/China Scholarship for Excellence.

References

- ABAQUS (2003), “ABAQUS Theory Manual, Version 6.7”, Hibbit, Karlsson and Sorensen Inc.
- ANSYS (2003), “ANSYS Multiphysics 10.0”, Canonsbury, Pennsylvania Inc.
- Barnett, T., Tizani, W. and Nethercot, D. (2001), “The practice of blind bolting connections to structural hollow sections: A review”, *Steel Compos. Struct., Int. J.*, **1**(1), 1-16.
- De Lima, L.R., L. Simoes da Silva, P.C. Vellasco and S.A. De Andrade (2004), “Experimental evaluation of extended endplate beam-to-column joints subjected to bending and axial force”, *Eng. Struct.*, **26**(10), 1333-1347.
- Ding, J. and Wang, Y.C. (2007), “Experimental study of structural fire behaviour of steel beam to concrete filled tubular column assemblies with different types of joints”, *Eng. Struct.*, **29**(12), 3485-3502.
- Comité Européen de Normalisation (2005), *CEN.EN1993-1-8, Eurocode 3: Design of steel structures, Part 1-8: Design of Joints*.
- Elghazouli, A.Y. and Izzuddin, B.A. (2000), “Response of idealised composite beam-slab systems under fire conditions”, *J. Construct. Steel Res.*, **56**(3), 199-224.
- Elghazouli, A.Y. and Izzuddin, B.A. (2001), “Analytical assessment of the structural performance of composite floors subject to compartment fires”, *Fire Safe. J.*, **36**(8), 769-793.
- Elghazouli, A.Y., Málaga-Chuquitaype, C., Castro, J.M. and Orton, A.H. (2009), “Experimental monotonic and cyclic behaviour of blind-bolted angle connections”, *Eng. Struct.*, **31**(11), 2540-2553.
- Faella, C., Piluso, V. and Rizzano, G. (2000), *Structural Steel Semi-Rigid Connections: Theory, Design and Software*, CRC Press, Florida, USA.
- France, J.E., Buick Davison, J. and Kirby, P.A. (1999), “Strength and rotational stiffness of simple connections to tubular columns using flowdrill connectors”, *J. Construct. Steel Res.*, **50**(1), 15-34.
- Ghobarah, A., Mourad, S. and Korol, R.M. (1996), “Moment-rotation relationship of blind bolted connections for HSS columns”, *J. Construct. Steel Res.*, **40**(1), 63-91.
- Gomes, F.C.T. (1996), “Moment capacity of beam-to-column minoraxis joints”, *Proceedings of IABSE International Colloquium on Semi-Rigid Structural Connections*, Istanbul, Turkey, IABSE: 319-326.
- Huck International Inc. (1990), *Industrial Fastening System*, Arizona, USA.
- Lee, J., Goldsworthy, H.M. and Gad, E.F. (2011), “Blind bolted moment connection to unfilled hollow section columns using extended T-stub with back face support”, *Eng. Struct.*, **33**(5), 1710-1722.
- Liu, T.C.H., Fahad, M.K. and Davies, J.M. (2002), “Experimental investigation of behaviour of axially restrained steel beams in fire”, *J. Construct. Steel Res.*, **58**(9), 1211-1230.
- Liu, Y. (2012), “Behaviour of steel connections under extreme loading conditions”, Ph.D. Thesis, Department of Civil and Environmental Engineering, Imperial College London, UK.
- Liu, Y., Málaga-Chuquitaype, C. and Elghazouli, A.Y. (2012a), “Response and component characterisation of semi-rigid connections to tubular columns under axial loads”, *Eng. Struct.*, **41**, 510-532.
- Liu, Y., Málaga-Chuquitaype, C. and Elghazouli, A.Y. (2012b), “Behaviour of beam-to-tubular column angle connections under shear loads”, *Eng. Struct.*, **42**, 434-456.
- Málaga-Chuquitaype, C. (2011), “Seismic behaviour and design of steel frames incorporating tubular members”, Ph.D. Thesis, Department of Civil and Environmental Engineering, Imperial College London, UK.
- Málaga-Chuquitaype, C. and Elghazouli, A.Y. (2010a), “Behaviour of combined channel/angle connections to tubular columns under monotonic and cyclic loading”, *Eng. Struct.*, **32**(6), 1600-1616.
- Málaga-Chuquitaype, C. and Elghazouli, A.Y. (2010b), “Component-based mechanical models for blind-bolted angle connections”, *Eng. Struct.*, **32**(10), 3048-3067.

- Park, A.Y. and Wang, Y.C. (2012), "Development of component stiffness equations for bolted connections to RHS columns", *J. Construct. Steel Res.*, **70**, 137-152.
- Pucinotti, R. (2001), "Top-and-seat and web angle connections: Prediction via mechanical model", *J. Construct. Steel Res.*, **57**(6), 661-694.
- Simoes da Silva, L., De Lima, L.R.O., Da S. Vellasco, P.C.G. and De Andrade, S.A.L. (2004), "Behaviour of flush endplate beam-to-bolumn joints under bending and axial force", *Steel Compos. Struct., Int. J.*, **4**(2), 77-94.
- Tizani, W., Wang, Z.Y. and Hajirasouliha, I. (2013), "Hysteretic performance of a new blind bolted connection to concrete filled columns under cyclic loading: An experimental investigation", *Eng. Struct.*, **46**, 535-546.
- Urbonas, K. and Daniunas, A. (2006), "Behaviour of semi-rigid steel beam-to-beam joints under bending and axial forces", *J. Construct. Steel Res.*, **62**(12), 1244-1249.
- Vlassis, A.G., Izzuddin, B.A., Elghazouli, A.Y. and Nethercot, D.A. (2008), "Progressive collapse of multi-storey buildings due to sudden column loss-Part II: Application", *Eng. Struct.*, **30**(5), 1424-1438.
- Vlassis, A.G., Izzuddin, B.A., Elghazouli, A.Y. and Nethercot, D.A. (2009), "Progressive collapse of multi-storey buildings due to failed floor impact", *Eng. Struct.*, **31**(7), 1522-1534.
- Wang, Z.Y., Tizani, W. and Wang, Q.Y. (2010), "Strength and initial stiffness of a blind-bolt connection based on the T-stub model", *Eng. Struct.*, **32**(9), 2505-2517.
- Yang, J.G., Murray, T.M. and Plaut, R.H. (2000), "Three-dimensional finite element analysis of double angle connections under tension and shear", *J. Construct. Steel Res.*, **54**(2), 227-244.
- Yeomans, N.F. (1998), *Rectangular Hollow Section Column using Lindapter Hollobolt*, (Choo and van der Vegte Eds.), Tubular Structures VIII, Rotterdam, Balkema, pp. 559-566.

DL

Appendix A: List of Notations

A_s	bolt cross sectional area
$A_{s,h}$	Hollo-bolt sleeve area
a	distance between the center of the bolt and column/channel surface
b_a	angle width
b_b	beam width
b_c	column/channel width
b_{eff}	angle effective width
C_c	coefficient for the calculation of K_{cfc}
C_t	coefficient for the calculation of K_{cft}
c	distance between the center of the bolt and the free edge of angle
d_b	bolt diameter
d_{M16}	diameter of M16 bolt
d_{bh}	bolt head diameter
d_0	bolt hole diameter
d	distance between the center of the bolt and beam flange surface
E	Young's Modulus
e_b	distance between the bolt row and the free edge of the plate
F_{ac}	compressive resistance of the angle component
F_{at}	tensile resistance of the angle component
F_{cfc}	compressive resistance of the channel/column component
F_{cft}	tensile resistance of the channel/column component
F_{bt}	tensile resistance of bolt
F_{st}	tensile resistance of standard bolt
F_{ht}	tensile resistance of Hollo-bolt
F_{bs}	bolt shear resistance
F_{ss}	shear resistance of standard bolt
F_{hs}	shear resistance of Hollo-bolt
F_{pb}	plate bearing resistance
F_{ab}	bearing resistance of angle leg
F_{bb}	bearing resistance of beam flange
F_{it}	tensile resistance of the i -th bolt row
F_t	tensile resistance of connection
F_c	compressive resistance of connection
$f_{y,a}$	angle yield stress
$f_{y,c}$	column/channel yield stress
$f_{u,b}$	bolt ultimate stress
$f_{u,h}$	ultimate stress of the Hollo-bolt sleeve
$f_{u,p}$	ultimate stress of the plate
f_{pry}	factor accounting for the change in the plastic hinge location in the leg of the angle component

h	beam height
i	bolt pitch dimension
K_{ac}	compressive stiffness of the angle component
K_{at}	tensile stiffness of the angle component
K_{cfc}	compressive stiffness of column/channel component
K_{cft}	tensile stiffness of column/channel component
k_{bt}	bolt tensile stiffness
K_{st}	tensile stiffness of standard bolt
K_{ht}	tensile stiffness of Hollo-bolt
k_{bs}	bolt shear stiffness
K_{ss}	shear stiffness of standard bolt
K_{hs}	shear stiffness of Hollo-bolt
K_b	bearing stiffness of plate
K_{ab}	plate bearing stiffness
K_{bb}	bearing stiffness of beam flange
K_{ic}	compressive stiffness of the i -th bolt row
K_{it}	tensile stiffness of the i -th bolt row
K_c	compressive stiffness of connection
K_t	tensile stiffness of connection
L	distance between Hollo-bolt centre and column/column edge
L_a	distance between beam flange and angle edge
L_b	bolt elongation length
L_c	distance between beam flange and column/channel free edge
M_{pl}	flexural capacity of angle leg
n_b	number of the bolts (column side)
n'_b	number of the bolts (beam side)
n_r	number of the bolt rows in tension
p_b	pitch of the bolt rows in the direction of load transfer
r_a	angle root radius
r_c	radius of column/channel root
t_a	angle thickness
t_c	column/channel thickness
t_p	plate thickness
ν	Poisson's ratio
δ	factor accounting for the punching resistance of column face
ε	factor accounting for the punching resistance of column face